Photo-gravitaxis in synthetic microswimmers

Dhruv P. Singh,[1,*] William E. Uspal,[1,2,*] Mihail N. Popescu,[1,2] Laurence Wilson,[3] and Peer Fischer[1,4]

[1] *Max-Planck-Institut für Intelligente Systeme, Heisenbergstr. 3, D-70569 Stuttgart, Germany*
[2] *IV. Institut für Theoretische Physik, Universität Stuttgart, Pfaffenwaldring 57, D-70569 Stuttgart, Germany*
[3] *Department of Physics, Univeristy of York, YO10 5DD Heslington, York, UK*
[4] *Institut für Physikalische Chemie, Universität Stuttgart, Pfaffenwaldring 57, D-70569 Stuttgart, Germany*

(Dated: November 3, 2017)

We have studied the dynamics of photo-chemically active colloids made out of silica cores half covered by successive thin layers of Ti and titania, respectively, and moving within aqueous peroxide solutions when exposed to ultra-violet (UV) light. The particles, initially sedimented at the bottom glass wall, exhibit wall-bound states of motion, dependent on the size of the particle, when illuminated from underneath the wall. Upon increasing the intensity of the UV light above a threshold value, which is also dependent on the size of the particle, the particles lift off the wall and move way from it, i.e., they exhibit a photo-gravitactic behavior bearing similarities with that of microorganisms such as phytoplankton and zooplankton. These dependencies on the particle size are rationalized by using a theoretical model of self-phoresis that explicitly accounts for the "shadowing" effect of the Ti/titania layers. This allows us to unequivocally identify the photochemical activity and phototactic response as the key mechanisms beyond the observed phenomenology. Consequently, one has the means to design photo-gravitatic particles that can reversibly switch between operating near a boundary or in the volume away from the boundary by judiciously adjusting the light intensity, i.e., simply by "turning a knob".

Keywords: phototaxis, Janus particles, self-propulsion, light-driven micromotors, artificial microswimmers

I. INTRODUCTION

Phototactic swimming against gravity is an interesting behavioral feature exhibited by a number of microorganisms like phytoplankton and zooplankton [1–4]. The photo-response to sunlight provides these swimmers with the ability to discern "up" from "down" in their choice of favorable living space: many of these species perform daily migration towards the upper layers of water to get more sunlight during the day, and then return to the lower layers during the night [1, 2, 5, 6]. Incorporating such photo- and gravi-tactic responses in synthetic swimmers holds the very promising feature of achieving well controlled, complex three-dimensional motion and precise positioning at various depths within a liquid layer.

For synthetic swimmers in the form of chemically active colloids, a gravitatic response can be achieved simply by "bottom heaviness" even for spherical shapes, as it has been shown by Ref. [7] and thoroughly analyzed theoretically in Ref. [8]. By employing particles with anisotropic shapes, e.g., L-shaped colloids with either the long or the short edge decorated by catalyst, a much more complex motion emerges: on an inclined surface, the particles exhibit both motion aligned with the direction of the gravity (the inclination of the plane) as well as perpendicular to it [9]. Additionally, in-plane phototactic response to light gradients, due to the chemical activity of the surface of the particle being proportional to the local intensity of light, has also been recently reported for the same carbon-silica particles in critical binary mixture [10] as well as for titania decorated particles in peroxide solutions [11].

It is clear that achieving motion against gravity requires that the particle align its direction of motion to have a component along the vertical. Additionally, its self-motility must be strong enough to overcome its sedimentation velocity (assuming that the particle is heavier than the suspending fluid). When the mechanism of propulsion is dependent on the intensity of light, achieving phototactic motion against gravity thus requires specific particle design and illumination conditions to allow the above conditions to be met. Here, we demonstrate experimentally that photo-gravitactic swimming can be achieved with light powered chemically active Janus particles that exhibit, additionally, a "geometrical shadowing" effect, in that only the part of catalyst directly exposed to light is active. We show that for sufficiently large light intensity, above certain threshold values that are dependent on the size of the particle, a lift-off from the surface occurs and the particles swim upward, away from the light source and against gravity, as schematically shown in Fig. 1(a). Furthermore, we show that for light intensity below the lift-off threshold, the particles exhibit a two-dimensional wall-bound motion; the exact nature of this wall-bound state is also dependent on the size of the particles. By employing the theoretical framework of self-phoresis [12, 13] and explicitly accounting for the "geometrical shadowing" effect, the size-dependent phenomenology revealed by the experiments is rationalized and the mechanisms behind it are identified. In particular, this allows us to unequivocally identify the

* corresponding authors: singh@is.mpg.de, uspal@is.mpg.de

photochemical activity and phototactic response, rather than bottom heaviness, as the key factors beyond the observed phenomenology. These findings provide an avenue for novel applications of chemically active colloids, in that one has the means to design photo-gravitatic particles that can, e.g., reversibly switch between operating near a boundary or in the volume away from the boundary by judiciously adjusting the light intensity. Additionally, for a polydisperse mixture of active particles, one could exploit the size-dependence of the lift-off threshold, tuning the light intensity to address particles in a specific size range and move them in or out of the boundary region.

II. RESULTS AND DISCUSSION

II.1. Photo-gravitactic swimming experiments

The light driven, self-propelled particles are fabricated by coating a hemisphere of spherical SiO_2 particles with a 5 nm film of metallic Ti followed up by a 50 nm anatase TiO_2 film (see Sect. IV for the details of the preparation process). A representative SEM image of the resulting silica-titania Janus particles is shown in Fig. 1(b), and the layered structure of the resulting particles is represented schematically in Fig. 1(c). We have investigated the motion of such chemically active colloids of two different sizes (radii $R = 0.5$ μm and 1.0 μm, respectively[1]) as a function of the light intensity of the UV illumination (see Sect. IV for the details about illumination conditions and experimental setup).

When dispersed in an aqueous hydrogen peroxide solution (2% H_2O_2, volume concentration), we observe that in the absence of illumination the particles sediment at the bottom wall and exhibit normal Brownian motion. As shown in Fig. 2 (a) and (e), neither the larger nor the smaller particles exhibit any pronounced bottom heaviness: the catalytic caps are at various orientations with respect to the wall, rather than predominantly facing down, towards the wall. This is in agreement with theoretical estimates [7, 14] based on employing the simple egg-shell model for the catalytic spherical cap [7]); for the Janus colloids described above (sizes and materials) suspended in the aqueous peroxide solution, the thermal equilibrium orientation of its symmetry axis exhibits a very weak preference (a potential well $\sim 1\ k_BT$, with k_B the Boltzmann constant and T the room temperature), for the catalytic cap "facing down".

Upon turning on the source of UV light (365 nm wavelength) located underneath the bottom glass wall, photo-catalytic decomposition of the peroxide at the titania covered surface proceeds according to the reaction

[1] The radius of the particle refers to the spherical core of silica, as provided by the manufacturer.

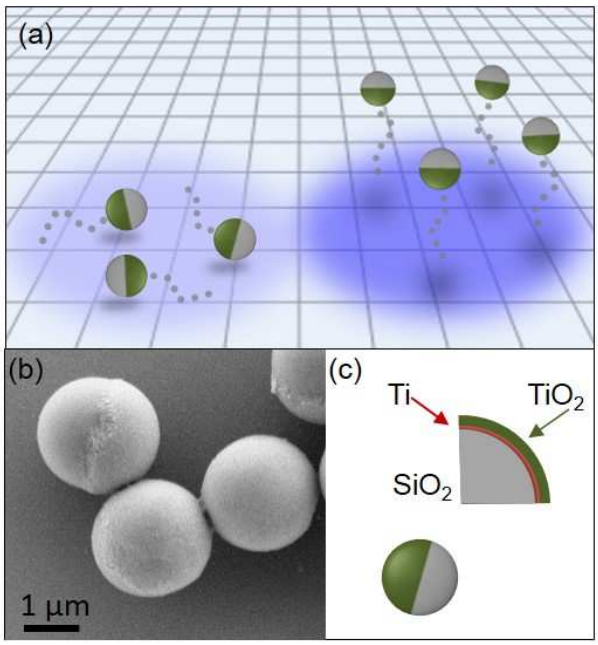

FIG. 1. a) Schematic drawing summarizing the main result of a transition from wall-bound two- dimensional motility of the photochemically active Janus particles at low intensity of light to a three-dimensional photo-gravitactic motion upon increasing the light intensity. The light and dark blue colors of the circular patches depict the cases of low and high intensity of light, the light-source being located beneath the bottom glass wall (depicted by the planar grid). b) SEM image of the silica-titania Janus particles showing the TiO_2 cap (in lighter gray) coated on top of the SiO_2 sphere. c) Schematic drawing depicting the layered structure of the photocatalytic cap.

scheme in Eqs. (1) [15–18]

$$TiO_2 + \hbar\omega \rightarrow h^+ + e^- \tag{1a}$$

$$H_2O_2 + 2h^+ \rightarrow O_2 + 2H^+ \tag{1b}$$

$$H_2O_2 + 2e^- + 2H^+ \rightarrow 2H_2O\,. \tag{1c}$$

Consequently, the solution around the particle is driven out of equilibrium and the gradients in chemical composition of the solution are expected to induce a self-phoretic motion of the particle [11, 14, 19–27]. Indeed, as shown in Fig. 2(b) and (c), we observe the particles setting in motion upon turning on the UV light source. However, in comparison to the previously reported in-plane phototactic motion [10, 11], a much richer swimming behavior is observed in our system. While at low and moderate values of the light intensity the particles exhibit a wall-bound, two-dimensional motion (Fig. 2(b) and (f)), we find that at sufficiently large light intensity, there is a "lift-off" transition: the particle swims into the bulk solution, *away* from the bottom wall. This is indicated by the out-of-focus diffuse rings in Fig. 2(c) and (g), and

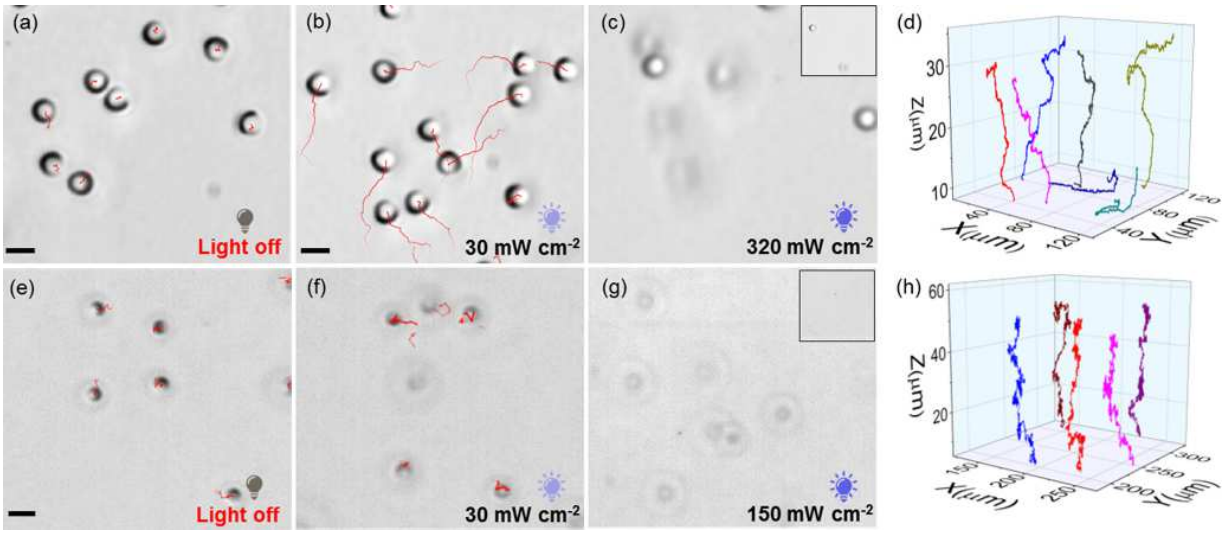

FIG. 2. (a)-(c) and (e)-(g): snapshots of the typical motion of photo-chemically active Janus particles at various values of the light intensities. (a)-(c) and (e)-(g) show the states for the larger (1 μm radius) and smaller (0.5 μm radius) size particles, respectively. The scale bar (same in all these panels) corresponds to 2 μm. (a),(e): Brownian motion of particles in the absence of illumination. (b),(f): typical motion at low to moderate light intensity; the larger particles exhibit a significant in plane motion away from the cap, evidenced by the 3 seconds back-tracked (past times) trajectories shown as red lines ending at the current positions on the particles, while the smaller particles exhibit a tendency of "cap down" orientation with small uplift from the surface. (c),(g): At large values of light intensity the particles move out of the wall, as shown by the out focused diffuse rings. The images show the state at 8 s after the light source was turned on. The insets in (c) and (g) show the state shortly after the snapshots in the main panels: almost all of the particles are now out of the focal plane.
(d),(h): three dimensional, persistent upward motion against gravity, for the smaller and larger particles, respectively. The trajectories shown are obtained by particle tracking using holographic microscopy and correspond to a 30 s observation time. Note that in (d) two instances of sliding followed by lift-off are captured (cyan and purple trajectories).

clearly confirmed by the three-dimensional trajectories, tracked by using holographic microscopy, shown in Fig. 2(d) and (h) (see also the video S0 in the Supporting Information (SI)).

By tracking the motion of the particles when they exhibit wall-bound, two-dimensional motion (Fig. 2(b) and (f)), it can be inferred that irrespective of their size the colloids move with the catalytic cap at the back ("away" from the catalyst). Furthermore, it can be seen in these figures that when in wall-bound states of motion, the particles exhibit a pronounced preference for certain orientations of the catalytic cap with respect to the wall. However, the exact details of the wall-bound motion seemingly depend on the size of the particle as follows.

For the larger size ($R = 1.0$ μm) particles, at low light intensity ($\lesssim 30$ mW $\times$ cm^{-2}) one observes motion predominantly along the wall (the red line trajectories shown in Fig. 2(b)), with occasional departures away from the wall of short time span and limited spatial extent. From the trajectories in Fig. 2(b), which correspond to a tracking duration of 3 s, one infers an average speed of 3.2 μm s^{-1} for the in-plane motion (see also the Video S1 in the SI). Upon gradually increasing the intensity of light, while the in-plane motion is still observed, it becomes apparent that frequently the orientation of the particle switches to "cap facing the wall". This is followed by (somewhat longer) excursions away from, but remaining close to, the wall, and then a return to the wall with consequent in-plane motion (see Video S2 in the SI). These features remain present for a wide range of values of the light intensity. Finally, at large values of the light intensity ($\gtrsim 200$ mW $\times$ cm^{-2}) the in-plane motion is no longer observed, but is replaced by a rapid lift-off of the particle from the wall. In Figure 2(c) we show an example of the lift-off from the wall as a snapshot of the motion at very large light intensity ($\gtrsim 320$ mW $\times$ cm^{-2}) taken very soon after the particles lift-off from the wall (the diffused black rings showing the particles that just moved out of the focus of the microscope objective, see also the Video S3 in the SI). The lift-off is now followed by a systematic reorientation of the cap to point towards the light source ("down") and persistent motion away from the wall (against gravity) for as long as the light source is on, as documented by the three-dimensional trajectories in Fig. 2(d) obtained via holographic microscopy (see Sec. IV for details of the holographic microscopy setup and measurements, and the video S0 in the SI).

For the smaller size ($R = 0.5$ μm) particles, the pattern of motion is distinctly different. At low light intensity, the particles exhibit large fluctuations in orientation, and no preferred orientation or significant directed motion is observed. Upon increasing the light intensity to values $\lesssim 30$ mW $\times$ cm^{-2}), one clearly observes a tendency of floating at some small height above the wall: the diffuse

images of the small particles shown in Fig. 2(f) indicate clearly that they are only slightly away from the focal plane (which coincides with the wall). The size of diffused rings and the change in the contrast of the particles image (see also the Video S4 in the SI) are indicative of the TiO_2 surface being oriented towards the bottom plane and of the particle being slightly away from the wall. Occasionally, short lived returns to the wall are observed, accompanied by slow motion along the wall (see the length of the trajectories (red lines) in Fig. 2(f)). Finally, at large values of the light intensity, similarly to the behavior of the larger particles, we observe complete lift-off from the surface and persistent motion away from the wall (source of light). Such a lift-off event at light intensity of 150 mW $\times$ cm^{-2} is shown in Fig. 2(g) (see also the Video S5 in the SI), while the persistent motion against gravity is documented by the three-dimensional trajectories in Fig. 2(h), obtained via holographic microscopy (see also the Video S0 in the SI).

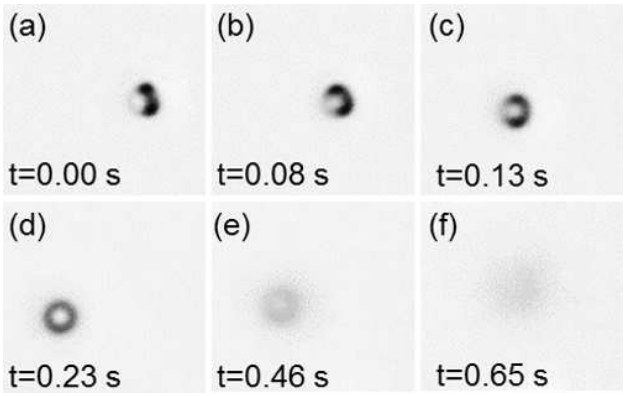

FIG. 3. High-speed camera captured reorientation and lift-off event for a small (0.5 μm radius) size Janus particle upon turning the light source on. (a) the state right before the light turned is turned on. (b)-(d) reorientation of the particle under the illumination, bringing the photo-chemically active cap "down", facing towards the light source. (e),(f) Once the particle reorients, it starts moving up: the diffuse images show that the particle is located away from the focal plane of the microscope, which coincides with the wall.

While it is known that swimming against the gravity can be achieved with bottom heavy Janus particles designed to move away from their denser catalytic caps [7], this is clearly not the case with our system. As discussed above (Fig. 2(a),(d)) bottom heaviness does not seem to be the effective feature and, furthermore, for the larger size particles it is evident that the orientation of the cap is rather determined by the light intensity. This motivated us to look also in more detail at the behavior of the smaller size particles at the onset of lift-off by using a high-speed camera. In Fig. 3 (a)-(f) we show the sequences of a typical lift-off event for a small particle, captured at high frame rate immediately after the light source is turned on (see also the Video S6 in the Supporting Information). These evidence a rapid response of the particle in that it rotates its catalytic cap towards the light, and then lifts off the surface. The observed reorientation time of ~ 0.23 s (see the time stamps in Fig. 3(a)-(d)) is approximately three times smaller than the rotational diffusion time ($\sim 0.76s$) of a Brownian particle of radius 0.5 μm in unbounded fluid; this strongly argues that the reorientation is being driven by light-source positioning and photo-catalytic activity rather than by the thermal fluctuations.

Summarizing the experimental observations, we have observed that for the photo-chemically active titania-silica Janus colloids there exists a size-dependent threshold light intensity above which the particles lift-off and move persistently upwards. This feature provides the means to address by size the particles in a polydisperse mixture and induce, for a fraction of them, motion in the volume, rather than on the surface; the process is reversible (decreasing the light intensity brings the particles back to the surface). Such a selective lift-off of the small size particles from the mixture of 0.5 and 1 μm radius particles is shown in the supplementary Video S7. Furthermore, below the threshold intensity, the in-plane motion as well as the orientation of the particles also show different characteristics for particles of different sizes: the larger size particles show significant sliding, while the smaller particles tend to orient "cap down" and float near the wall. To understand the mechanisms beyond this phenomenology, and in particular the dependencies of the size of the particles, in the next section we develop and study a theoretical model of self-phoresis that explicitly accounts for the "shadowing" effect of the Ti/titania layers. The issue of the three-dimensional motion after the lift-off, which required dedicated experimental studies as well as an involved theoretical analysis properly accounting for the effect of thermal fluctuations, will be presented elsewhere [28].

II.2. Theoretical model

The model we consider for a light-activated catalytic Janus particle in the vicinity of a planar wall is as follow. The spherical particle of radius R is half-covered by catalyst, and its orientation is defined by the vector $\hat{\mathbf{d}}$ laying along the axis of the symmetry and pointing from the catalytic pole to the inert pole. The center of the sphere, $\mathbf{x}_p = (x_p(t), y_p(t), z_p(t))$, is at height $h = z_p$ above a (transparent) planar wall located at $z = 0$, and the particle orientation vector $\hat{\mathbf{d}}$ makes an angle θ with respect to the normal vector to the wall, which is in the $\hat{z}$ direction (see Fig. 4). The system is illuminated from beneath the (transparent) wall and the particle is "opaque" to light; therefore, for $\theta = 180°$ the catalytic cap of the particle faces away from the wall and is completely in shadow, while for $\theta = 0°$, the entire catalytic cap is illuminated. Considering for the moment the dynamics in the absence of thermal fluctuations, we can assume without loss of generality that the vector $\hat{\mathbf{d}}$ is in the xz plane.

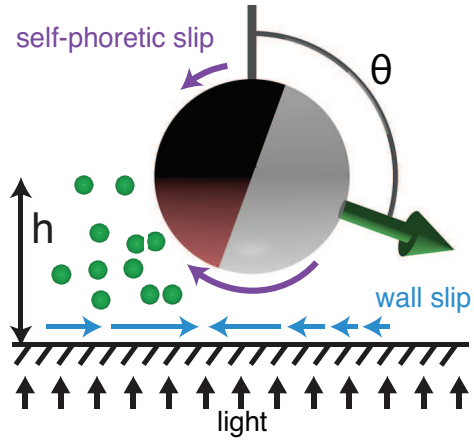

FIG. 4. Schematic depiction of a spherical, photo-chemically active Janus particle located near a planar wall. The center of the particle is at height h above the wall, and the orientation $\hat{\mathbf{d}}$ of the particle makes an angle θ with the normal $\hat{z}$ to the wall.The system is illuminated from underneath the plane and the particle is "opaque" to light (geometric shadowing), which is illustrated by the two colors on the catalytic cap: brown for the illuminated region, and black for the shadowed region. Chemical reactions at the illuminated catalyst lead to release of solute molecules (shown as tiny green disks) into the surrounding solution. Gradients of solute concentration drive self-diffusiophoretic slip on the surface particle, as well as chemi-osmotic slip on the planar wall. Self-propulsion of the particle with translational and rotational velocities $\mathbf{U}$ and $\mathbf{\Omega}$, respectively, emerges.

We will model the active motion of the colloid within the classical framework of neutral diffusiophoreis [12, 13]. In brief, the illuminated region of the catalytic face of the particle creates product molecules ("solute"), and the gradient in solute density along the surface of the particle induces a phoretic slip, which drives the motion of the particle with translational and rotational velocities $\mathbf{U}$ and $\mathbf{\Omega}$, respectively. The detailed mathematical formulation of our model is provided in Sec. IV.4. We note here that similarly simple models have been successfully employed to capture the experimentally observed emergence of sliding along walls, cross-stream migration, or motion guided by topographical patterns [14, 26, 29, 30].

Irrespective of the presence of the wall, the motion of the particle in general results from the interplay of 1.) particle weight (i.e., sedimentation), 2.) bottom-heaviness, and 3.) light-induced activity, each of them defining a characteristic velocity.

1. The particle weight (i.e., buoyancy) can be characterized by a sedimentation velocity V^s. This velocity is calculated for an inactive particle in free space (i.e., far away from bounding surfaces.) depending on the geometry of the particle, its material composition, etc.

2. The catalytic cap of the particle is associated with bottom-heaviness, due to its weight and displacement from the particle center. Bottom-heaviness introduces a gravitational torque $\tau^{bh} \sim \tau_0^{bh} \sin\theta$, and hence can be characterized by the maximum rotational velocity of a particle in free space, $\Omega_0^{bh} = \tau_0^{bh}/8\pi\eta R^3$.

3. The quantity $U^{\mathrm{d,fs}}$ is the velocity of an active particle with a completely illuminated cap ($\theta = 0°$) that is far away from bounding surfaces (i.e., is in ***f***ree ***s***pace). Additionally, for the purpose of this definition, the particle is assumed to be neutrally buoyant (i.e., has the same density as the suspending fluid) and not bottom-heavy. Under these conditions, the particle will move in the $\hat{\mathbf{d}}$ direction (i.e., along the axis of symmetry) with $d\theta/dt = 0$.

Therefore, we first seek to characterize the relative importance of the three effects. By expressing the velocities in units of V^s, the other two characteristic velocities above introduce two dimensionless parameters. The first is the bottom-heaviness parameter G:

$$G \equiv \frac{\Omega_0^{bh} R}{V^s}. \tag{2}$$

It is important to note that this parameter is size dependent. In general, the total weight of the particle will scale as R^3, where R is the radius of the particle. Since the Stokes drag coefficient of the particle scales as R, the sedimentation velocity $V^s \sim R^2$. The characteristic torque from bottom-heaviness τ_0^{bh} is due to the weight of a cap with area $\sim R^2$ and thickness t (where $t << R$), as well as the displacement $\sim (R+t) \approx R$ of the cap center of mass from the particle center, such that $\tau_0^{bh} \sim R^3$. Therefore, $\Omega_0^{bh} \sim R^0$, i.e., Ω_0^{bh} has a negligible dependence on R. Accordingly, we find that $G \sim R^{-1}$, and therefore the value of G will vary between the experiments with particles of different sizes. The experimentally relevant range of values for G can be estimated as follows. We recall that the light-activated particles employed in this study have a "double film" structure. The first layer has a thickness $t_1 = 5\,\mathrm{nm}$ and is composed of Ti, which has a density of $\rho_{\mathrm{Ti}} \approx 4.5 \times 10^3\,\mathrm{kg/m^3}$. The second layer has a thickness $t_2 = 50\,\mathrm{nm}$ and is composed of titania, which has a density of $\rho_{\mathrm{TiO_2}} \approx 3.78 \times 10^3\,\mathrm{kg/m^3}$. Seeking only a rough estimate of G, we make the simplifying assumption of replacing the structure above with a single layer of effective density $\rho_{cap} \approx 4000\,\mathrm{kg/m^3}$ and effective thickness $t = 55\,\mathrm{nm}$, with the "eggshell" geometry (cap thickness varies smoothly from zero at the particle "equator" to a maximum at the catalytic "pole") proposed by Ref. [7]. This leads to values $G \approx 0.1$ for an $R = 0.5\,\mu\mathrm{m}$ particle, and $G \approx 0.05$ for a $R = 1\,\mu\mathrm{m}$ particle.

The second dimensionless parameter A characterizes activity:

$$A \equiv \frac{U^{\mathrm{d,fs}}}{V^s}. \tag{3}$$

This parameter is very difficult to calculate *a priori*, particularly since it requires knowledge of the exact interactions with the particle for each of the molecular species in the solution [12]. Moreover, the velocity of a particle observed in typical experimental conditions (e.g., a particle moving near a substrate) will not be the same as $U^{\mathrm{d,fs}}$, recalling the definition of $U^{\mathrm{d,fs}}$ given above. However, progress can be made by assuming that the experimentally observed near-wall velocities and $U^{\mathrm{d,fs}}$ are of the same order of magnitude. Hence, $U^{\mathrm{d,fs}} \sim 1\,\mu$m/s to $20\,\mu$m/s, depending on the light intensity and other conditions. Since a typical value of V^s is $V^s \sim 3\,\mu$m/s, we arrive at the conclusion that A, as a free parameter, may vary between typical values of $A = 0.1$ (low light intensity) and $A = 10$ (high light intensity).

With these estimates, we are now in position to employ the model and study the influence of the size of the particle and of the light intensity on the emerging dynamics.

II.3. Theoretical analysis

We study theoretically the phenomenology for the two sizes of particle employed in the experiment upon increasing the light intensity and we show here that the model captures the main features of the experimental phenomenology for the two sizes. In the language of our model, analyzing the dynamics of a particle of given size as a function of the light intensity translates to fixing the bottom-heaviness parameter G, i.e., $G = 0.1$ for the smaller particles and $G = 0.05$ for the larger ones, while varying the activity parameter A, which encodes the effect of light intensity, in the experimentally relevant range $0.1 \leq A \leq 10$ (low to high intensity). For a given light intensity A, the behavior of a particle is compactly summarized by a phase portrait showing the evolution of the particle height h and orientation θ from any initial h_0 and θ_0.

In Fig. 5, we show the phase portraits for a small particle corresponding to value $A = 0.2$, $A = 0.5$, and $A = 0.8$, i.e., low, moderate, and high light intensity, respectively. For low intensity, the particle is attracted to a "cap-down" steady state (green circle) in which the particle hovers at a steady height h^* above the wall, with its cap pointing directly towards the wall ($\theta^* = 0°$). The "cap-down" orientation of the particle and the solute concentration around the particle in a hovering state is depicted in Fig. 6. At the steady height h^*, the contribution of swimming activity to the vertical velocity is exactly balanced by particle heaviness (i.e., the sedimentation velocity.) The stability of this state against perturbations to the particle height can be understood from straightforward arguments. Due to the presence of the hard, impenetrable wall, the concentration of solute molecules in the space between the cap and the wall is enriched, relative to the concentration for a particle in unbounded liquid. The concentration gradient on the surface of the particle s, accordingly, enhanced, leading

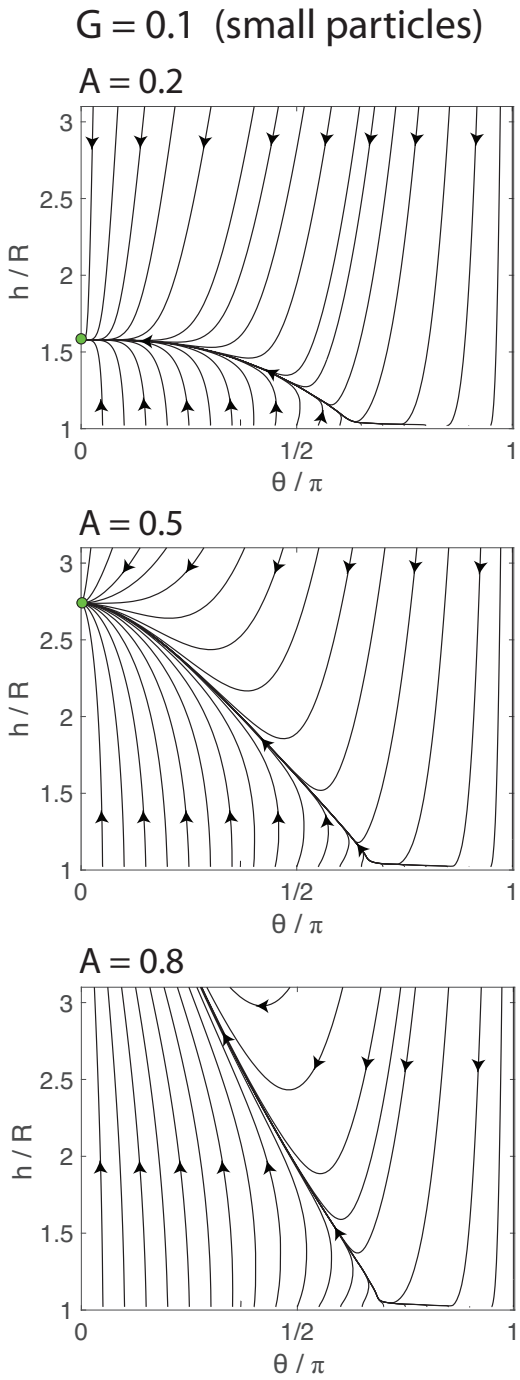

FIG. 5. Phase portraits for small particles ($G = 0.1$) for various activity parameters A. All other parameters are as given in the text. Green circles indicate attractors.

to a higher swimming velocity than the bulk value $U^{d,fs}$. If the particle is perturbed to a height below h^*, the solute confinement effect is enhanced; the swimming velocity becomes larger than the sedimentation velocity, and the particle moves away from the wall. If, instead, the particle is perturbed to a height $h > h^*$, the solute

confinement effect is weakened, the swimming velocity becomes less than the sedimentation velocity, and the particle moves towards the wall.

The "cap-down" steady state noticed above is also stable against perturbations of the orientation of the particle, i.e., small changes in the angle θ away from $\theta = 0°$. There are several effects that contribute to the angular velocity of a particle. We have previously discussed bottom-heaviness. Our model also includes rotation by solute gradients, i.e., phoretic rotation. This effect arises due to the material difference between the two faces of the particle, which, in the framework of our model, translates into a contrast of phoretic mobilities (Sec. IV.4). We note here that we have chosen the parameters of our model to recover the experimental observation that particles rotate their catalytic face towards the source of light. Therefore, both bottom-heaviness and phoretic rotation drive rotation of the particle cap towards $\theta = 0°$.

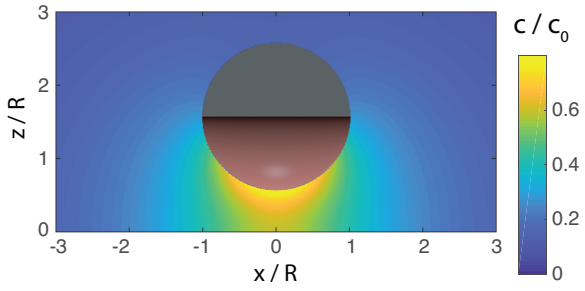

FIG. 6. Concentration field around a small particle in a "hovering" state with $A = 0.2$. The particle height and orientation are $h^*/R = 1.5$ and $\theta^* = 0°$, respectively. The concentration is scaled by the characteristic concentration $c_0 \equiv \kappa R/D$.

Now we consider the dynamics at $A = 0.5$, i.e., moderate light intensity. The particle is still attracted to a cap-down steady state, but this state has shifted to a larger height h^*, due to the faster swimming velocity of the particle. If A is increased even further to $A = 0.8$, there is no longer any steady state in range of heights ($1.02 < h/R \leq 3.1$) considered. For all initial heights and orientations, the particle leaves the vicinity of the wall.[2] This behavior agrees with the expectation that once $A \approx 1$, i.e., once the swimming velocity becomes larger than the sedimentation velocity, the particle will be able to overcome the effect of gravity and swim away from the wall.

We now turn to the case of the larger size particles ($G = 0.05$), which exhibits a much richer phenomenology as shown by the phase portraits in Fig. 7. At low intensity ($A = 0.2$), there is a cap-down attractor, but it is bistable with a "sliding" state. In a sliding state, the particle maintains a steady orientation $\theta^* \approx 90°$ and height h^* and swims along the wall. The solute concentration around a sliding particle is depicted in Fig. 8(a). As the light intensity is increased to moderate values (e.g., $A = 0.5$), the cap-down state shifts towards higher values of h^*, but the sliding state remains in roughly the same position. For even larger values of the light intensity (e.g., $A = 0.8$), the cap-down attractor disappears, but the sliding state persists; in fact, the sliding state is robust for a broad range of A. At very high light intensities, above a critical threshold $A_c \approx 2.1$, the sliding state attractor disappears. Therefore, for $A > A_c$, the particle will leave the vicinity of the wall for any initial height and orientation. Surprisingly, the particle can swim away from the surface even for some orientations $\theta > 90°$, i.e., with the cap tilted away from the wall. This result highlights the role of the shadowing in the dynamics of a particle: as illustrated in Fig. 8(b) the particle tends to swim away from the illuminated area of the cap, instead of away from the catalytic pole.

As discussed in connection with the small particles, bottom-heaviness and phoretic rotation both tend to drive the particle towards a cap-down orientation, $\theta = 0°$. Therefore, to explain the emergence of a stable angle $\theta \approx 90°$ for large particles, there must be other significant contributions to the angular velocity. Our model includes hydrodynamic interactions with the wall that are induced by the swimming activity of the particle. In brief, by swimming, the particle generates flows in the surrounding solution. These flows scatter off the wall, coupling back to the particle and contributing to the rotation [31]. Additionally, our model includes chemi-osmotic surface flows driven on the wall by particle-generated solute gradients. These chemi-osmotic surface flows drive flow in the bulk solution, coupling back to the particle. For large particles, the effect of bottom-heaviness is small enough ($G = 0.05$) for a stable orientation $\theta \approx 90°$ to emerge from the interplay of phoretic rotation, bottom-heaviness, hydrodynamic interactions, and chemi-osmotic wall slip.

In summary, the predictions of our theoretical model – a cap-down state for small particles, and the emergence of a sliding state for large particles – capture the most significant features of the experimental observations. In agreement with the experimental observations of clear qualitative distinction between the behaviors of small and large particles, the model predicts that the small particles "hover" above the wall at low light intensities, and swim away at high light intensities. Large particles are observed in the experiments to swim along the wall, and occasionally leave the vicinity of the wall, for a broad range of light intensities. This behavior corresponds to the bistable dynamics predicted by our theory. Finally, at high light intensities the dynamical attractors disappear, and the flows in the corresponding phase plots imply that the large particles also swim away from the wall,

[2] From the diagram, it can be seen that if the particle is initially oriented towards the wall, i.e., $\theta \approx 180°$, the particle "crashes" into the wall, i.e., the particle height passes below the lower cutoff for our numerical calculations, $h/R = 1.02$. We have confirmed that if we include a short-ranged repulsive potential between the particle and the wall, these trajectories do indeed leave the wall.

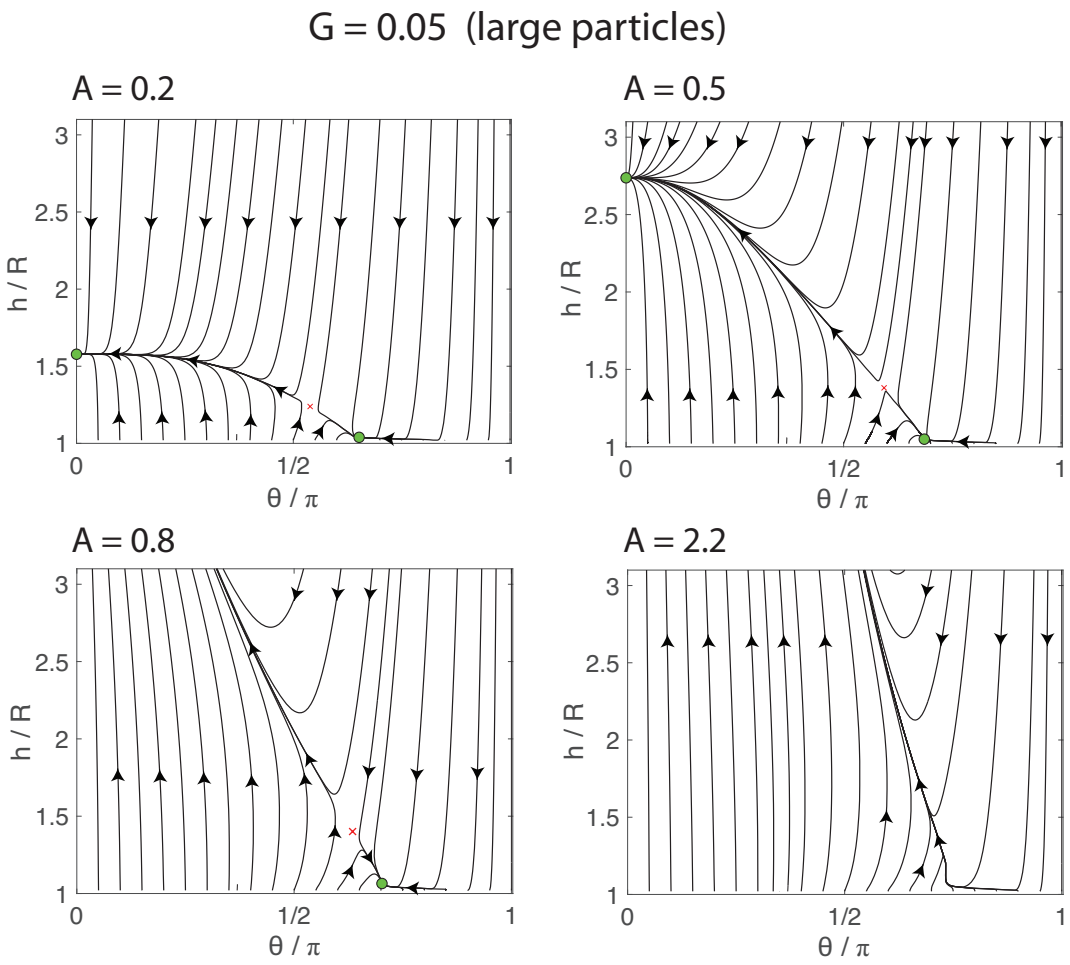

FIG. 7. Phase portraits for large particles ($G = 0.05$) for various activity parameters A. All other parameters are as given in the text. Green circles indicate attractors. Red crosses indicate saddle points.

as observed in the experiments at high light intensities.

We end this section with a brief comment on the fact that the theoretical framework employed is deterministic and does not incorporate the effects of thermal fluctuations. It is reasonable to ask whether the dynamical attractors are robust against thermal noise. This question can be most straightforwardly addressed in terms of the Péclet number of the particle, Pe, defined as $Pe \equiv V^s R/D_T$ (where $D_T = k_B T/6\pi\eta R$ is the translational diffusion coefficient of a particle in free space), which characterizes the significance of thermal noise: i.e., noisy systems have a small Péclet number. Since $V^s \sim R^2$, as discussed above, Pe is a strongly size-dependent quantity: $Pe \sim R^4$. For the small particles, we estimate $Pe \approx 1$, and for the large particles, $Pe \approx 15$. These values indicate that the small particles will exhibit strong fluctuations around the cap-down state, which explains why this state is difficult to identify in an experiment, while large particles will exhibit only moderate fluctuations around the bistable cap-down and sliding states.

III. CONCLUSIONS

We have studied experimentally and theoretically the motion of photo-chemically active, spherical Janus particles made out of silica cores and half covered with a Ti/titania bilayer upon UV illumination. We have experimentally demonstrated that photo-gravitactic swimming can be achieved with these light powered Janus particles: for sufficiently large light intensity, above certain threshold values that are dependent on the size of the particle, the particles lift-off from the surface and swim upward, away from the light source and against gravity. Furthermore, we have evidenced that for light intensity below the lift-off threshold, the motion of small and large particles near the wall exhibit qualitatively different behaviors. By using a theoretical model within the framework of self-diffusiophoresis, we have captured both the size-dependence of the lift-off threshold intensity, as well as the qualitatively different behavior below the threshold intensity. The small particles "hover" above the wall at

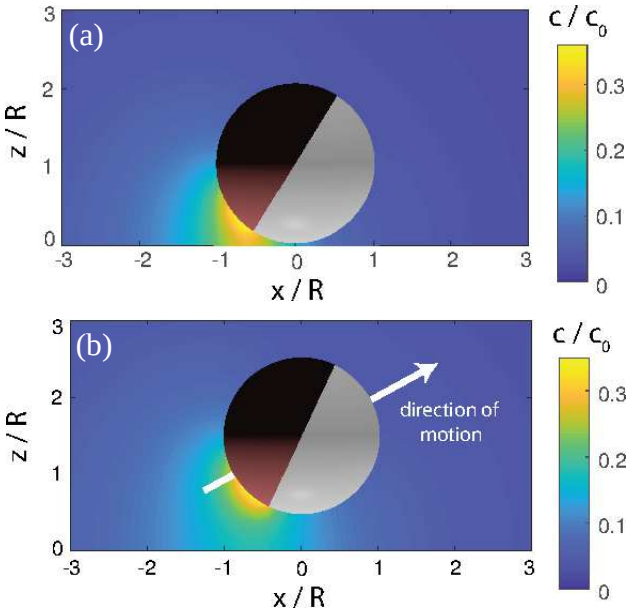

FIG. 8. (a) Concentration field around a large particle in a "sliding" state with $A = 0.5$. (b) Concentration field around a large particle taking off from the surface with $A = 2.2$. The particle height and orientation are $h/R = 1.5$ and $\theta = 115°$, respectively. Although the cap is tilted slightly away form the wall, the particle can still leave the surface, since its direction of motion is directed approximately away from the illuminated area of the cap. In both cases, the concentration is scaled by the characteristic concentration $c_0 \equiv \kappa R/D$. Here, we might include a figure panel showing a lift-off trajectory

low light intensities, while the large particles exhibit a bistable dynamics (sliding and hovering), as experimentally observed.

The results of our study provide an avenue for novel applications of chemically active colloids based on designing photo-gravitatic particles. For example, such particles can reversibly switch between operating near a boundary or in the volume away from the boundary by judiciously adjusting the light intensity, and polydisperse mixture of active particles can be addressed in specific size ranges for movement in or out of the boundary region.

IV. METHODS AND MATERIALS

IV.1. Fabrication of light-driven Janus Particles

The light driven active Janus particles were prepared by coating of anatase phase TiO_2 thin film over commercial (micromod) SiO_2 microspheres (0.5 and 1 μm radius) as follows. First, a monolayer of SiO_2 particles was formed on a Si substrate by using a standard Langmuir-Blodgett method [32]. The substrate with the monolayer of particles was transferred to the chamber of a vapor deposition system and a 5 nm film of titanium (Ti), subsequently followed by a 50 nm film of TiO_2, was deposited on the particles by using e-beam evaporation at normal incidence. The Ti film, which adheres very well to the SiO_2 surface, provides a significantly improved adhesion for the TiO_2 film as compared to the one of the SiO_2 surface. The as-deposited TiO_2 film is amorphous; therefore, the phase transformation from amorphous to the photo-active anatase phase has been induced by annealing the Janus particles at 450 °C for two hours in air [18]. In the final step, the Janus particles so fabricated were detached from the substrate by sonication in water.

IV.2. Illumination and particle tracking

For each experiment, a small volume of the aqueous suspension with Janus particles of the desired size is mixed with a corresponding volume (for a 2 % volume concentration) of peroxide solution immediately prior to the start of the experiment. A sessile droplet of the mixture is formed on a plasma-cleaned glass cover slip, in air, and the particles are allowed to sediment. The drop is imaged from underneath by using a microscope with a a 63X objective in an inverted geometry, and the image acquisition is performed at 10 to 100 frames per seconds. The particles are set in motion by UV illumination. A 365 nm UV light emitting diode was used to illuminate the sample through the objective lens in an epifluorescence-type set-up. The simultaneous imaging is performed with white light in transmittance mode by using a set of beam splitter and filters which reject the UV light while allowing white light coming from top of the sample to reach the camera. The maximum UV intensity in the sample plane that could be achieved in this set-up was 320 mW $\times$ cm^{-2}. The particle tracking in the video recordings of the experiment was subsequently performed using the ImageJ distribution Fiji and the plugin TrackMate [33].

IV.3. Particle tracking in three dimensions

For three-dimensional motion, particle tracking was achieved by employing digital inline holographic microscopy (DIHM). This method has previously been used to track, among other things, microscopic particles [34, 35] and microorganisms [36–38]. Our optical setup is built around an inverted optical microscope, and has been described in more detail elsewhere [38]. The key modification to a standard bright-field configuration was made by replacing the illumination system with a single-mode optical fiber, coupled to a laser diode (wavelength 642 nm). The fiber is terminated with a free-space coupler, which directs light on to the sample. Particles in the sample scatter some of the incident light, which interferes with the unscattered light to form a hologram at the image plane. The hologram image was captured by a CMOS sensor (Mikrotron MC-1362) with a resolution of 1024 $\times$ 1024 pixels at a frame rate of 100 Hz.

Each experimental run consisted of eight uncompressed video sequences, 2800 frames in length. Two types samples were imaged: particles of radius 0.5 μm, using a 20x objective lens (a notional pixel size of 0.708 μm); and particles of radius 1.0 μm, using a 100x oil immersion objective lens (yielding a pixel size of 0.14 μm). The latter was chosen to allow the high optical power density, of approximately 300 mW $\times$ cm^{-2} in the sample plane, necessary in order to achieve photo-gravitaxis of the larger (and thus heavier) particles. Volumetric data was reconstructed from each instantaneous hologram by using the Rayleigh-Sommerfeld back-propagation scheme [39], and a method based on the Gouy phase anomaly [40] was used to locate particles within this volume. Particle tracks were assembled by correlating the positions of the particles in subsequent frames.

IV.4. Mathematical formulation of the model

The geometry of the system is as specified in Sect. II.2. The model we use for the dynamics of a light-activated catalytic Janus particle is defined as follows. Over the illuminated region of the catalytic face of the particle, there is an outward flux of product molecules ("solute") that is locally proportional to the flux of incident light. The solute number density field $c(\mathbf{x})$ is governed by the Laplace equation, $D\nabla^2 c(\mathbf{x}) = 0$, where $\mathbf{x}$ is a point in the liquid solution, and D is the diffusion coefficient of the solute molecules. The boundary condition on the solute number density field is $-D\left[\hat{\boldsymbol{n}}\cdot\nabla c\right] = \kappa\left(\hat{\boldsymbol{n}}\cdot\hat{z}\right)\Theta(-\hat{\boldsymbol{n}}\cdot\hat{z})\,\Theta(-\hat{\boldsymbol{n}}\cdot\hat{d})$ over the surface of the particle, and $-D\left[\hat{\boldsymbol{n}}\cdot\nabla c\right] = 0$ on the wall. Here, $\Theta(x)$ is the Heaviside step function, and the local surface normal $\hat{\mathbf{n}}$ is defined to point from the surface into the liquid solution. In the boundary condition on the particle surface, the first step function represents the condition that only illuminated areas produce solute, while the second step function represents the condition that this only occurs on the catalytic cap. Additionally, the solute number density field decays to a constant value c^∞ far away from the particle. The solute production rate κ is some function of the light intensity I, $\kappa = \kappa(I)$, with $\kappa(0) = 0$; we assume, as suggested by the experimental observation, that $\kappa(I)$ is a monotonously increasing function. We note that this model of light-activated solute production is similar to the one of Cohen and Golestanian [41], here applied to Janus particles instead of particles with a uniform surface chemistry.

In order to model propulsion driven by solute gradients, we employ the classical theory of neutral self-diffusiophoresis [12, 13, 19]. The suspending fluid is an incompressible Newtonian liquid with mass density ρ and dynamic viscosity η. We assume small Reynolds number $Re \equiv \rho V^s R/\eta$, so the fluid velocity $\mathbf{u}(\mathbf{x})$ and pressure $P(\mathbf{x})$ are governed by the Stokes equation $-\nabla P + \eta\nabla^2\mathbf{u} = 0$ and the incompressibility condition $\nabla\cdot\mathbf{u} = 0$. The interaction of the solute molecules with a bounding solid surface (i.e., the wall or one of the particle faces) drives a surface flow that is modeled by an effective slip velocity $\mathbf{v}_s(\mathbf{x}_s) = -b(\mathbf{x}_s)\nabla_{||}c(\mathbf{x})|_{\mathbf{x}=\mathbf{x}_s}$. Here, $\mathbf{x}_s$ is a point on a bounding surface, $\nabla_{||} \equiv (\mathbf{I} - \hat{\boldsymbol{n}}\hat{\boldsymbol{n}})\cdot\nabla$, and $b(\mathbf{x}_s)$ is a material dependent parameter (the so-called "surface" or "phoretic" mobility) that encapsulates the molecular details of the interaction between the solute and the surface. We note that $b < 0$ represents an effective repulsive interaction, and $b > 0$ represents an effective attractive interaction. The fluid velocity obeys the boundary conditions $\mathbf{u}|_{\mathbf{x}=\mathbf{x}_s} = \mathbf{U} + \boldsymbol{\Omega}\times(\mathbf{x}_s - \mathbf{x}_p) + \mathbf{v}_s(\mathbf{x}_s)$ on the particle surface and $\mathbf{u}|_{\mathbf{x}=\mathbf{x}_s} = \mathbf{v}_s(\mathbf{x}_s)$ on the wall. Here, $\mathbf{U}$ and $\boldsymbol{\Omega}$ are the (yet unknown) translational and angular velocities of the particle, respectively. Additionally, the fluid is quiescent far away from the particle, i.e., $\mathbf{v}(|\mathbf{x} - \mathbf{x}_p| \to \infty) = 0$. To close the system of equations for $\mathbf{U}$ and $\boldsymbol{\Omega}$, we write a force balance equation, $\int \boldsymbol{\sigma}\cdot\hat{\boldsymbol{n}}\, dS = -\mathbf{F}^g$ and a torque balance equation, $\int (\mathbf{x}_s - \mathbf{x}_p)\times\boldsymbol{\sigma}\cdot\hat{\boldsymbol{n}}\, dS = -\boldsymbol{\tau}^{bh}$, with the integrals taken over the surface of the particle. Here, $\mathbf{F}^g$ is the buoyancy force on the particle, $\boldsymbol{\tau}^{bh}$ is the torque due to bottom-heaviness, and $\boldsymbol{\sigma} \equiv -P\mathbf{I} + \eta\left[\nabla\mathbf{u} + \nabla^T\mathbf{u}\right]$ is the stress tensor for a Newtonian liquid.

We take the surface mobility $b(\mathbf{x}_s)$ to be piecewise uniform, so that $b(\mathbf{x}_s) = b_{cap}$ over the catayltic cap, $b(\mathbf{x}_s) = b_{inert}$ over the inert face of the particle, and $b(\mathbf{x}_s) = b_w$ on the wall. Based on the experimental observations, we seek to estimate reasonable values for these parameters. First, noting that the inert face and the wall are both made of silica, we assume $b_{inert} = b_w$. Secondly, we recall the definition of $U^{\mathrm{d,fs}}$ given above. Analytically, it can be shown that for this model,

$$\frac{U^{\mathrm{d,fs}}}{U_0} \approx -\frac{\mathrm{sgn}(b_{cap})}{12}\left(1 + \frac{b_{inert}}{b_{cap}}\right) - \mathrm{sgn}(b_{cap})\frac{1447}{32768}\left(1 - \frac{b_{inert}}{b_{cap}}\right), \qquad (4)$$

with the quantity $U_0 \equiv \frac{|b_{cap}|\kappa}{D}$ [28].
Since the particle moves away from its catalytic cap in free space, we require $U^{\mathrm{d,fs}} > 0$. This places certain bounds on b_{inert} and b_{cap}: either (i.) $b_{cap} < 0$ (the cap has a repulsive interaction with the solute) and $b_{inert}/b_{cap} > -3.3$, (ii.) or $b_{cap} > 0$ (the cap has an attractive interaction with the solute) and $b_{inert}/b_{cap} < -3.3$.

Furthermore, we note that in the experiment the particles are observed to rotate their caps to face the light when they are in bulk solution. Since this alignment strengthens with increasing light intensity, it is not simply an effect of bottom-heaviness, but is also driven by catalytic activity.[3] This phoretic rotation can be captured within our model by a surface mobility contrast, $b_{cap} \neq b_{inert}$. It can be shown (we omit the details for

[3] As previously remarked, a detailed analysis of the three dimensional motion of the light activated particles is in progress and it will be published elsewhere.

brevity) that the observed alignment of the cap towards the light entails either (iii.) $b_{cap} < 0$ and $b_{inert}/b_{cap} > 1$, or (iv.) $b_{cap} > 0$ and $b_{inert}/b_{cap} < 1$.

Choosing the more restrictive conditions from (i) and (iii), and from (ii) and (iv), we conclude that either (A.) $b_{cap} > 0$ and $b_{inert}/b_{cap} < -3.3$ or (B.) $b_{cap} < 0$ and $b_{inert}/b_{cap} > 1$. Now we consider condition (A). In this case, there is a very strong surface mobility contrast, and hence very strong phoretic rotation. We find that, in this case, phoretic rotation dominates other effects that induce particle rotation, and always drives θ to $\theta = 0°$. Therefore, the experimentally observed "sliding" state of larger particles cannot be reproduced if the parameters are chosen according to (A). Consequently, we choose condition (B), with a modest surface mobility contrast $b_{inert}/b_{cap} \gtrapprox 1$ that does not overwhelm other contributions to particle rotation; in particular, we assume $b_{inert}/b_{cap} = 1.1$. Since the inert core and the catalytic cap are both oxide materials, it is indeed reasonable to suppose that they have similar molecular interaction potentials with the solute, and hence similar surface mobilities.

Finally, we recall that we chose V^s as a characteristic velocity scale, and that we represent the effects of activity and bottom-heaviness by the non-dimensional parameters A and G, respectively. Accordingly, we set $\mathbf{F}^g = -6\pi\eta R V^s \hat{z}$, which ensures that $\mathbf{U} = -V^s\hat{z}$ when the light is turned off and the particle is far away from the wall ($h/R \gg 1$). In order to introduce G into the model, we set $\boldsymbol{\tau}^{bh} = -8\pi\eta R^2 G V^s \sin(\theta)\hat{y}$, as implied by Eq. (2). At this point, the only unspecified parameters are b_{cap}, D, and κ. From Eq. (4) (see also, e.g., Refs. [29, 30]), it can be inferred that the contribution of activity to the generalized velocity $(\mathbf{U}, \boldsymbol{\Omega})$ of the particle is proportional to the quantity $U_0 = \frac{|b_{cap}|\kappa}{D}$. Therefore, it is not necessary to specify b_{cap}, D, and κ individually, but only their in the combination U_0. Combining Eqs. (3) and (4) for $b_{cap} < 0$ and $b_{inert}/b_{cap} = 1.1$, we find that $U_0 \approx 0.17\, A\, V^s$.

SUPPORTING INFORMATION

Supporting Information is available online from the Wiley Online Library or from the author.

ACKNOWLEDGMENTS

This work was supported by the DFG as part of the project SPP 1726 117 (microswimmers, FI 1966/1-1), and the Max Planck Society.

[1] D.-P. Häder, Arch. Microbiol. **147**, 179 (1987).
[2] B. Eggersdorfer and D.-P. Häder, FEMS Microbiol. Lett. **85**, 319 (1987).
[3] G. B. Witman, Trends Cell Biol. **3**, 403 (1993).
[4] G. Jékely, J. Colombelli, H. Hausen, K. Guy, E. Stelzer, F. Nédélec, and D. Arendt, Nature **456**, 395 (2008).
[5] C. S. Yentsch, R. H. Backus, and A. Wing, Limnol. Oceanogr. **9**, 519 (1964).
[6] R. B. Forward, in Photochemical and Photobiological Reviews Vol. 1, edited by K. Smith (Springer, Boston, MA, 1976) p. 157.
[7] A. Campbell and S. J. Ebbens, Langmuir **29**, 14066 (2013).
[8] K. Wolff, A. M. Hahn, and H. Stark, Eur. Phys. J. E **36**, 43 (2013).
[9] B. ten Hagen, F. Kümmel, R. Wittkowski, D. Takagi, H. Löwen, and C. Bechinger, Nat. Commun. **5**, 4829 (2014).
[10] C. Lozano, B. ten Hagen, H. Löwen, and C. Bechinger, Nat. Commun. **7**, 12828 (2016).
[11] C. Chen, F. Mou, L. Xu, S. Wang, J. Guan, Z. Feng, Q. Wang, L. Kong, W. Li, J. Wang, and Q. Zhang, Adv. Mater. **29**, 1603374 (2017).
[12] J. L. Anderson, Ann. Rev. Fluid Mech. **21**, 61 (1989).
[13] R. Golestanian, T. B. Liverpool, and A. Ajdari, New J. Phys. **9**, 126 (2007).
[14] J. Simmchen, J. Katuri, W. E. Uspal, M. N. Popescu, M. Tasinkevych, and S. Sánchez, Nat. Commun. **7**, 10598 (2016).
[15] F. Mou, Y. Li, C. Chen, W. Li, Y. Yin, H. Ma, and J. Guan, Small **11**, 2564 (2015).
[16] I. Ilisz, K. Föglein, and A. Dombi, J. Mol. Catal. Chem. **135**, 55 (1998).
[17] P. Salvador and F. Decker, J. Phys. Chem. **88**, 6116 (1984).
[18] D. P. Singh, U. Choudhury, P. Fischer, and A. G. Mark, Adv. Mater. **28**, 1701328 (2017).
[19] R. Golestanian, T. B. Liverpool, and A. Ajdari, Phys. Rev. Lett. **94**, 220801 (2005).
[20] J. R. Howse, R. A. L. Jones, A. J. Ryan, T. Gough, R. Vafabakhsh, and R. Golestanian, Phys. Rev. Lett. **99**, 048102 (2007).
[21] R. Dong, Q. Zhang, W. Gao, A. Pei, and B. Ren, ACS Nano **10**, 839 (2016).
[22] F. Mou, L. Kong, C. Chen, Z. Chen, L. Xu, and J. Guan, Nanoscale **8**, 4976 (2016).
[23] J. G. Gibbs and Y. Zhao, Small **6**, 1656 (2010).
[24] J. Palacci, S. Sacanna, A. P. Steinberg, D. J. Pine, and P. M. Chaikin, Science **339**, 936 (2013).
[25] A. Brown and W. Poon, Soft Matter **10**, 4016 (2014).
[26] S. Das, A. Garg, A. I. Campbell, J. Howse, A. Sen, D. Velegol, R. Golestanian, and S. J. Ebbens, Nat. Commun. **6**, 8999 (2015).
[27] S. Ebbens, D. A. Gregory, G. Dunderdale, J. R. Howse, Y. Ibrahim, T. B. Liverpool, and R. Golestanian, Eur. Phys. Lett. **106**, 58003 (2014).
[28] S. P. Dhruv, W. E. Uspal, M. N. Popescu, L. Wilson, and P. Fischer, *in preparation* (2017).
[29] W. E. Uspal, M. N. Popescu, S. Dietrich, and M. Tasinkevych, Soft Matter **11**, 434 (2015).
[30] J. Katuri, W. E. Uspal, J. Simmchen, A. Miguel-López, and S. Sánchez, arXiv:1706.06817 (2017).

[31] S. E. Spagnolie and E. Lauga, J. Fluid Mech. **700**, 105 (2012).
[32] D. Schamel, M. Pfeifer, J. G. Gibbs, C. Miksch, A. G. Mark, and P. Fischer, J. Am. Chem. Soc. **135**, 12353 (2013).
[33] C. A. Schneider, W. S. Rasband, and K. W. Eliceri, Nat. Methods **9**, 671 (2012).
[34] J. Sheng, E. Malkiel, and J. Katz, Appl. Opt. **45**, 3893 (2006).
[35] F. C. Cheong, B. J. Krishnatreya, and D. G. Grier, Opt. Express **18**, 13563 (2010).
[36] J. Sheng, E. Malkiel, J. Katz, J. Adolf, R. Belas, and A. R. Place, Proc. Natl. Acad. Sci. **104**, 17512 (2007).
[37] F. Saglimbeni, S. Bianchi, A. Lepore, and R. Di Leonardo, Opt. Express **22**, 13710 (2014).
[38] J. F. Jikeli, L. Alvarez, B. M. Friedrich, L. G. Wilson, R. Pascal, R. Colin, M. Pichlo, A. Rennhack, C. Brenker, and U. B. Kaupp, Nat. Commun. **6**, 7985 (2015).
[39] S.-H. Lee and D. G. Grier, Opt. Express **15**, 1505 (2007).
[40] L. Wilson and R. Zhang, Opt. Express **20**, 16735 (2012).
[41] J. A. Cohen and R. Golestanian, Phys. Rev. Lett. **112**, 068302 (2014).